Scaffold-free and scaffold-assisted 3D culture enhances differentiation of bone marrow stromal cells

Prasanna Vidyasekar[1] · Pavithra Shyamsunder[1] · Sanjeeb Kumar Sahoo[2] ·
Rama Shanker Verma[1,3]

Abstract 3D cultures of stem cells can preserve differentiation potential or increase the efficiency of methods that induce differentiation. Mouse bone marrow-derived stromal cells (BMSCs) were cultured in 3D as scaffold-free spheroids or "mesoid bodies" (MBs) and as aggregates on poly(lactic) acid microspheres (MB/MS). 3D cultures demonstrated viable cells, interaction on multiple planes, altered cell morphology, and the formation of structures similar to epithelial cell bridges. Cell proliferation was limited in suspension cultures of MB and MB/MS; however, cells regained proliferative capacity when transferred to flat substrates of tissue culture plates (TCPs). Expanded as monolayer, cells retained expression of Sca-1 and CD44 stem cell markers. 3D cultures demonstrated enhanced potential for adipogenic and osteogenic differentiation showing higher triglyceride accumulation and robust mineralization in comparison with TCP cultures. Enhanced and efficient adipogenesis was also observed in 3D cultures generated in a rotating cell culture system. Preservation of multilineage potential of BMSC was demonstrated in 5-azacytidine treatment of 3D cultures and TCP by expression of cardiac markers GATA4 and ACTA1 although functioning cardiomyocytes were not derived.

Introduction

Standard cell culture is 2D where cells on a flat substrate do not have the cell–cell interaction or cell–matrix interaction found in vivo (Yamada and Cukierman 2007). The 3D environment of an organ affects cell function and cell fate as several critical cellular processes are influenced by the surrounding microenvironment (Bloom and Zaman 2014). Therefore, in vitro culture of cells in 3D can help in understanding authentic, in vivo cellular function and differentiation. The morphology of cells and intercellular signaling is more physiological in 3D cultures than in standard 2D cell cultures. Furthermore, 3D cell cultures permit rapid experimental manipulations using molecular biology techniques and allow better imaging by microscopy than animals (Yamada and Cukierman 2007). Sphere formation by cells in suspension allows a high degree of multiplanar interactions between cells and cell matrix and the formation of niches and microenvironments. Embryonic stem cells form spheroids termed embryoid bodies that can be differentiated to cardiomyocytes (Lei et al. 2015), and spheroids of cancer cells called tumorospheres serve as intermediate cancer models between in vitro cancer cell lines and in vivo tumors (Weiswald et al. 2015). Cell spheroids are therefore basic but effective tools to create 3D environments and can be generated using static suspensions or agitating bioreactors. The 3D spheroid culture model can also be applied to adult stem cells (Baraniak and McDevitt 2012; Cha et al. 2015). Bone marrow stromal cells (BMSCs) or

✉ Rama Shanker Verma
vermars@iitm.ac.in

[1] Stem Cell and Molecular Biology Laboratory, Department of Biotechnology, Bhupat and Jyoti Mehta School of Biosciences, Indian Institute of Technology Madras, Chennai 600 036, India

[2] Institute of Life Sciences, Nalco Square, Bhubaneswar 751023, India

[3] Department of Biotechnology, Bhupat and Jyoti Mehta School of Biosciences, Indian Institute of Technology Madras, Chennai 600036, Tamil Nadu, India

MSC possess the ability to self-renew and differentiate to a number of mesenchymal lineages in vitro (Pittenger 2008). Undifferentiated BMSC can either be transplanted in vivo into region of trauma where in situ differentiation can occur, or differentiated BMSC can be expanded in vitro and transplanted. Both methods require a considerable number of BMSC, which are often expanded by standard cell culture in tissue culture plates (TCPs) prior to transplantation. However, the plasticity of BMSC reduces with the prolonged culture that is required to generate cell numbers suitable for transplantation because multiple passages and long-term cultures tend to lose self-renewal, replication, and differentiation potential (Bonab *et al.* 2006; Wagner *et al.* 2010). Culturing MSC in spheroids has been reported to preserve their multilineage potential (Baraniak and McDevitt 2012; Cha *et al.* 2015). In this study, we explore the effects of spheroid culture on "mesoid bodies" (MBs) of BMSC using scaffold-free and scaffold-assisted modes of culture. Mesoid bodies were grown on poly(lactic acid) (PLA) microspheres (MB/MS) and scaffold-free culture using static suspensions (MB). We report the changes in adipogenic, osteogenic, and cardiomyogenic differentiation of MB and MB/MS in comparison to standard 2D culture in TCP. We also explore the use of the rotating cell culture system (RCCS) to develop a protocol for efficient differentiation of BMSC into adipocytes.

Materials and Methods

Isolation and culture of MSCs. Swiss albino (SA) mice were procured from King's Institute, Chennai, Tamil Nadu, India. All procedures were approved by the Institutional Animal Ethics Committee (IIT Madras, India) and the Committee for the Purpose of Control and Supervision of Experiments on Animals (CPCSEA), Government of India. *Standard 48-h culture protocol*: Adult SA mice (6-wk old and above) were sacrificed by cervical dislocation, and femur and tibia were dissected out in ice-cold Dulbecco's phosphate-buffered saline (DPBSA) using iris or Castroviejo Scissors. The marrow cavity was exposed at both ends using a vascular forceps and surgical scalpel (BP handle 4, size 20). A 27-gauge needle attached to a 10-ml syringe containing ice-cold media was inserted into the spongy bone exposed by removal of the growth plate to flush out the marrow. Bone marrow cells were centrifuged at $80\times g$ and replated in a TCP containing Dulbecco's modified Eagle's medium-F12 (DMEM/F12) supplemented with 10% fetal bovine serum (FBS), 100 U/ml penicillin, 100 μg/ml streptomycin, 2 mM L-glutamine, 1 mM sodium pyruvate, and 0.1 mM non-essential amino acids (Life Technologies, Carlsbad, CA). Cells were seeded at a density of 2.5×10^6 cells/ml and incubated at 37°C, 5% CO_2 in a humidified incubator. Non-attached cells were removed with change of medium after 48 h. *Modified protocol*:

Adult SA mice less than 3 wk old and 25 g in weight were used for isolation of bone marrow cells, and procedures were carried out in complete medium which was prewarmed to 37°C. Flushed marrow was passed through a 100-μ filter mesh (BD Biosciences, Bedford, MA) before plating as described above. After 3 h, the non-adherent cells were removed gently and medium was replenished. Medium was changed every 8 h for 72 h of culture. Confluent cells were passaged by washing with DPBSA, followed by incubation in 0.5 ml of 0.25% trypsin/EDTA (Life Technologies) for 2 min at room temperature. After neutralization with complete medium, cells were centrifuged and replated in fresh TCP at a ratio of 1:2.

Spheroid culture of BMSC. Scaffold-free cultures were generated by using up to 0.5×10^6/ml of enzymatically dissociated BMSC that formed mesoid bodies in suspension over a 2% agar underlay on TCP surface within 48 h. Scaffold-assisted cultures were generated similarly using microspheres provided by Dr. Sanjeeb K Sahoo, Institute of Life Sciences, Bhubaneswar. Porous PLA microspheres co-polymerized with gelatin, alginate, dextran, and pectin were prepared by modifying the solvent evaporation method as previously reported by Sahoo et al. (2005). Twenty milligrams of lyophilized microspheres was suspended in FBS for 1 h prior to culture. Enzymatically dissociated cells (0.5×10^6) were mixed with microspheres gently and incubated for up to 48 h for cells to adhere and aggregate to form MB/MS. MB and MB/MS were shifted from suspension to TCP surface using 1-ml pipettes.

Immunocytochemistry. Immunocytochemistry (ICC) for cell markers was carried out as reported previously (Tekkatte *et al.* 2012), by using primary antibodies against anti-alpha sarcomeric actin (ACTA1; 1:100; raised in mouse; Sigma-Aldrich, St. Louis, MO), Sca-1 (1:100 raised in mouse; Santa Cruz Biotechnology, Santa Cruz, CA), CD44 (1:50; raised in rat; Santa Cruz Biotechnology), Thy1 (1:50; raised in mouse; Santa Cruz Biotechnology), CD29 (1:50; raised in mouse; Santa Cruz Biotechnology), GATA4 (1:100; raised in mouse; Santa Cruz Biotechnology), CD34 (1:100; raised in rat; Santa Cruz Biotechnology) after the cell monolayer had been fixed in 4% paraformaldehyde (PFA) and 0.25% Triton-X. Nuclei were stained with 4′,6-diamidino-2-phenylindole (DAPI) (1:500 from a 2 mg/ml stock; Sigma-Aldrich). The samples were subsequently incubated with fluorescein isothiocyanate (FITC)-conjugated anti-rat/mouse IgG (1:100; Sigma-Aldrich) for 1 h at room temperature. Finally, cells were washed well in DPBSA and visualized by using a fluorescence microscope (Nikon TiE, Melville, NY, with NIS Elements Nikon Advanced Research (Ars) 3.0 imaging software).

Live staining with DiI. The progression of growth around microspheres was visualized by staining the cells with a carbocyanine dye, 1,1′-dioctadecyl-3,3,3′,3′-tetramethylindocarbocyanine perchlorate (DiI). One milliliter of fresh DMEM/F12 was added along with 8 ml of 5 mg/ml DiI (40 mg/ml) to a BMSC monolayer, and the flasks were incubated at 37°C overnight. Cells were washed well and enzymatically dissociated with trypsin/EDTA. DiI-loaded cells were seeded on microspheres as previously described and incubated. The stained cells were visualized using Nikon-Ti fluorescent microscope using a TRITC (Texas Red) filter. Perimeter and area of fluorescent MB/MS were calculated using the Nikon Ar (Advanced Research) Software algorithm for measurement.

Scanning electron microscopy. Cultures were washed and fixed in 4% glutaraldehyde at room temperature for 45 min followed by washes in DPBSA. Cultures were then subjected to a series of alcohol washes using 40, 60, 80, 90, and 100% ethanol, for less than a minute in each dilution. Dried samples were visualized using a FEI Quanta 200 scanning electron microscope with secondary electron (SE) and back-scattered electron (BSE) detectors. Carbon sputtering was carried out if samples necessitated the need for definition during imaging.

Semiquantative RT-PCR and RT-PCR amplification. RNA was isolated using Trizol reagent (Sigma-Aldrich), and 1.5 μg of total RNA was converted to complementary DNA (cDNA) using MMLV-RT (Thermo Scientific, Waltham, MA) and oligo-dT primers (New England Biolabs, Beverly, MA). The resulting cDNA was amplified by PCR using gene-specific primers. PCR products were visualized on a 2.5% agarose gel after staining with ethidium bromide. Real-time PCR was carried out as previously reported (Shyamsunder *et al.* 2013) using SYBR Green Real-Time PCR Kit from Qiagen on an Eppendorf Mastercycler, ep realplex (Eppendorf, Hamburg, Germany). Relative mRNA expression was determined by normalization to the expression of a housekeeping gene, beta-actin (primer list is provided in Supplementary Table 1, densitometry analysis for SQRT-PCR was carried using ImageJ software).

Western blotting. Western blotting was carried out as previously reported (Shyamsunder *et al.* 2013). Cells were washed with phosphate-buffered saline (PBS), lysed in ice-cold radio immunoprecipitation assay (RIPA) lysis buffer containing protease inhibitors and centrifuged at $10,000 \times g$ for 15 min at 4°C to remove debris. Protein concentration in the cell lysates was estimated using the BCA method (Pierce, Madison, WI). The protein samples were mixed with 1× Laemmli sample buffer and boiled for 5 min. Proteins were subjected to 10% SDS-PAGE and electroblotted onto Bio-Rad, 0.22-μM nitrocellulose membrane (Bio-Rad Laboratories, Hercules, CA). Primary antibodies for GATA4

(1:150; Santa Cruz Biotechnology), alpha sarcomeric actin (ACTA1; 1:500; Sigma-Aldrich), and beta actin (ACTB; 1:1000; Sigma-Aldrich) were used along with goat anti-rabbit and anti-mouse horseradish peroxidase-conjugated secondary antibodies (1:10,000; Sigma-Aldrich). Antibody-reactive proteins were detected by means of enhanced chemiluminescence, Pierce ECL Plus western blotting detection reagents (Pierce). The chemiluminescence intensity was captured using VersaDoc Imaging System (Bio-Rad). Densitometry analysis for WB was carried using ImageJ software.

Flow cytometry for surface marker analysis and cell cycle. Cells were fixed in 4% PFA and labeled with anti-Sca-1, CD44, Thy-1, and CD105 mAb (anti-mouse, raised in rat; BD Biosciences) for 45 min. Cells were then washed with DPBSA three times and labeled with FITC-conjugated anti-rat IgG mAb (Sigma-Aldrich). Labeled cells were analyzed with a flow cytometer (Becton, Dickinson FACSCalibur, San Jose, CA). Gating was implemented based on unlabelled and FITC-conjugated IgG isotype control staining profiles. For cell cycle analysis, the cells were harvested and washed in PBS before fixation in cold 70% ethanol which was added drop wise to the pellet while vortexing. Cells were fixed for 30 min at 4°C. Fixed cells were washed twice in PBS and spun at $250 \times g$ in a centrifuge. Cells were incubated with 50 μl of a 100 μg/ml stock of RNase and 200 μl propidium iodide (from 50 μg/ml stock solution). A BD FACSCalibur flow cytometer was used to analyze the cell population for cell cycle changes.

Adipogenic, osteogenic, and cardiomyogenic differentiation. The adipogenesis induction medium consisting of 500 μM 3-isobutyl-1-methylxanthine (IBMX), 10 μM indomethacin, and 1 μM dexamethasone in DMEM/F12 with 10% FBS and osteogenic medium consisted of 0.2 mM ascorbic acid, and 10 mM β-glycerophosphate in DMEM/F12 10% FBS was applied to scaffold-free and scaffold-assisted cultures of BMSC. The medium was changed every 48 h. Cardiomyogenic differentiation was carried out by administering 5 μM 5-azacytidine for 24 h. Cells were washed well with DPBSA and replenished with fresh DMEM/F12. Cells were observed for morphological changes for 32 days from day of 5-azacytidine (5-aza) treatment.

Oil red staining and Nile red staining for mature adipocytes. Oil Red O stock was prepared with 0.03 g of Oil Red O dissolved in 10 ml of 100% isopropanol. Working solution of Oil Red O (ORO) was freshly prepared by adding 6 ml of the ORO stock solution to 4 ml of distilled water and kept at 40°C for 1 h and filtered. Cells fixed in 10% formalin for 30 min at room temperature (RT) were rinsed well with distilled water before adding ORO working solution and kept for 15 min at RT. The stain was removed and washed with

DPBSA followed by subsequent washes in milliQ water. The adipogenic-differentiated cells with the triglyceride droplets were visualized and identified by characteristic round shape and intracellular lipid accumulation, stained bright red by ORO. To perform the quantification of triglyceride accumulation, Oil Red O was solubilized by treating the stained cells with 100% isopropanol for 10 min. With the eluted sample, the optical density was measured with a spectrophotometer at 520 nm (PerkinElmer, Waltham, MA). For Nile red staining, cells were fixed for 30 min in 10% neutral-buffered formalin at room temperature and washed twice with PBS. Cells were then incubated for 15 min with 8 mg/ml DAPI and 1 mg/ml Nile red in PBS at room temperature. Cells were washed and visualized with a fluorescence microscope.

CFU assay. Cells were cultured in methyl cellulose at 10× of final concentration (0.3 ml of cells to 3 ml of methyl cellulose). A thin layer of methyl cellulose cell mixture was dispensed using a 3cc syringe and evenly spread in the dish by gentle swirling. Cultures were incubated at 37°C, 5% CO_2 in air, and ≥95% humidity. Attached cells formed colonies that were then stained with crystal violet (0.5 mg/ml in 1% methanol) for 20 min and air-dried after washing in distilled water. Stained colonies were visualized under a Nikon eclipse Ti phase contrast microscope.

BrdU labeling for cell proliferation. Bromodeoxyuridine (BrdU; Sigma-Aldrich) was diluted to a 1 mM concentration with 1× DPBS, and 50 μl of 1 mM stock was added to expanded cells from MB (final concentration is 10 μM of BrdU). Cells were incubated at 37°C with 5% CO_2 in air for 1 h before visualization with a florescence microscope.

Statistical analysis. All experiments were carried out in replicates, and results were expressed as mean±SD. Statistical significance was calculated by using Student's *t* test with the Prism 5 program (GraphPad Software, San Diego, CA).

Results and Discussion

Culture of BMSC in 2D monolayer and 3D suspensions. The adult bone marrow stromal cell can be cultured in vitro in basal media under standard culture conditions. Under adequate conditions, these cells can differentiate into the various lineages of mesenchymal origin. BMSC were isolated from the femur and tibia of adult Swiss albino mice and cultured in TCPs (Soleimani and Nadri 2009) as a monolayer. Isolation and culture conditions were optimized to generate cultures that contained Sca-1^{+}, CD44^{+}, CD29^{+}, CD90^{+}, CD105^{+}, and CD34^{−} cells (Fig. 1a–k). The expression of these markers indicates a multipotent, progenitor cell population. The ability of BMSC to adhere to plastic is vital to their culture as a monolayer (Fig. 2a) and is a minimal criterion for identification as a mesenchymal stem cell (Dominici *et al.* 2006). Under specific conditions (Spheroid culture of BMSC section), BMSC can be cultured in static suspensions as aggregates of cells by providing an unsuitable surface for adherence (Fig. 2b). These scaffold-free aggregates were termed MBs in reference to their highly potent embryonic stem cell counterparts, embryoid bodies, generated with similar methods (Itskovitz-Eldor *et al.* 2000). Based on the method of aggregation, MB ranged in size from 20 μm in diameter to over 200 μm. Culture conditions were optimized such that typical MB would be between 50 and 100 μm in diameter (Fig. 2b). When the same aggregation method was used in the presence of PLA MS (Fig. 2c), the MB adhered to the MS, incorporating multiple MS into large aggregates (Fig. 2d) and proliferated around them, using the MS effectively as scaffolds. The MB/MS aggregates could then be transferred to a TCP where, similar to explant cultures, the cells were shed from the MB/MS onto the TCP surface and proliferated as a monolayer
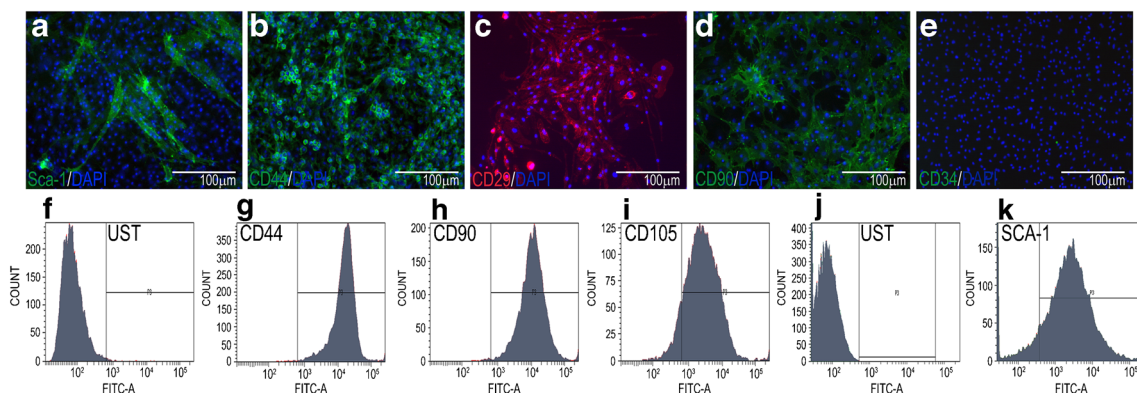

Figure 1. Characterization of BMSC. (*a–e*) Characterization of MSC by ICC for surface markers Sca-1^{+}, CD44^{+}, CD29^{+}, CD90^{+}, and CD34^{−}, respectively (nuclei counterstained with DAPI). (*f–k*) Flow cytometry analysis of MSC markers CD44, CD90, and CD105 with unstained control (*f–i*) and Sca-1 with UST (unstained) control (*j, k*).
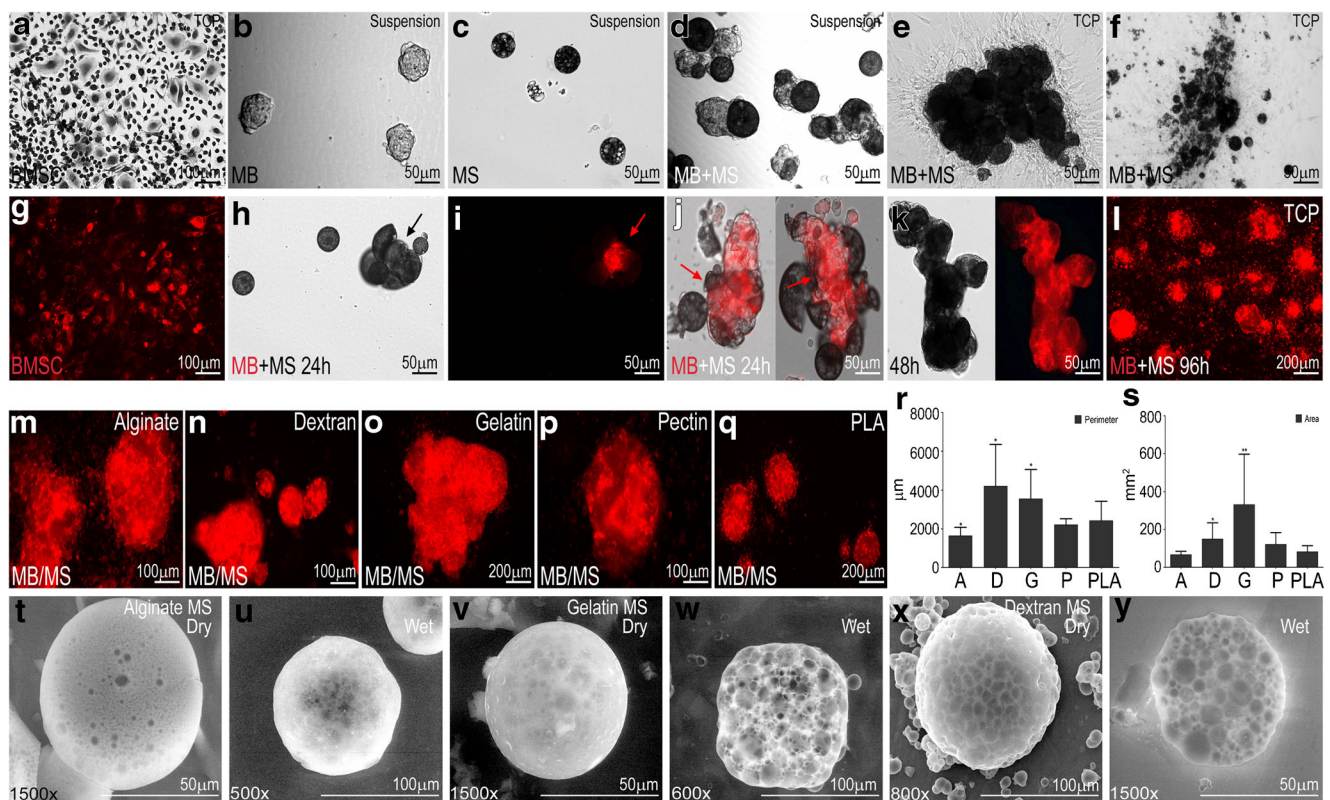
Figure 2. Culture of BMSC as MB and MB/MS. The figure describes 3D culture of BMSC as mesoid bodies (MBs) and as aggregates with microspheres (MB/MS). Live staining was used to confirm viability and growth of cells around microspheres and their aggregation. (*a*) Crystal violet stained monolayer culture of BMSC. (*b*) BMSC grown in suspension as MB. (*c*) Bright field micrograph of microsphere (MS) in suspension. (*d*) Cells grown as MB on MS (MB/MS). MB incorporates multiple MS and proliferates using them as scaffolds. (*e*) Cells shed from MB/MS and expanded as a monolayer on TCP. (*f*) MS degraded by confluent growth of BMSC. (*g*) DiI stained (live) BMSC in TCP. (*h*) BF micrograph showing an MB/MS in stages of formation at 24 h. Cells are loaded with DiI. (*i*) Fluorescent micrograph showing DiI-loaded BMSC incorporating MS. (*j*) Merged image showing progressive incorporation of multiple MS and MB, forming large aggregates. (*k*) DiI staining demonstrates confluent MB/MS aggregate in 48 h where microspheres are completely incorporated and encapsulated within MB/MS. (*l*) DiI-loaded MB/MS transferred to TCP after 48 h and grown as monolayer for further 48 h. (*m*–*q*) Co-polymerization of PLA MS for MB/MS culture. PLA was co-polymerized with different substances to increase cell adhesion and growth on MS. (*m*–*q*) DiI-loaded MB cultured on alginate-PLA, dextran-PLA, gelatin-PLA, pectin-PLA, and only PLA microspheres. (*r*, *s*) Perimeter and area comparison, respectively, between MB/MS cultures using Nikon Ar automated florescence-based measurement tool (*A* alginate, *D* dextran, *G* gelatin, *P* pectin); *p value 0.01 to 0.05, **p value 0.001 to 0.01, ***p value 0.0001 to 0.001. (*t*–*y*) Scanning electron micrographs show surface and shape of alginate, gelatin, and dextran—PLA MS under dry and wet conditions. Difference in porosity can be observed.

(Fig. 2*e*). Over a period of 10–14 days, the cells formed a confluent monolayer and detached from the scaffolds, degrading them in the process (Fig. 2*f*). The degraded MS were washed out during routine maintenance and subculture.

The microspheres are solid particles, and therefore, detailed visualization of cell growth around the MB/MS was carried out using a live imaging procedure with a fluorescent dye. DiI is a lipophilic carbocyanine dye and is used for live tracking of MSC in vivo (Weir *et al.* 2008). The dye uniformly labels cells via lateral diffusion in the plasma membrane without affecting cell viability, development, or basic physiological properties. Figure 2*g* shows a live monolayer of BMSC stained with DiI. Stained cells were trypsinized and cultured along with microspheres to generate fluorescent MB/MS aggregates (Fig. 2*h*, *i*). As the fluorescent signal is exclusive to the cells, the pattern and growth of cells on MB/MS can be observed under a fluorescent microscope. Figure 2*h*, *i*, *j* demonstrates initial incorporation of MS into MB aggregates over brief time periods (~24 h) where microspheres are clearly distinguishable. Figure 2*k* shows a confluent MB/MS aggregate where the microspheres are completely engulfed by cell growth after ~48 h. The dye is retained after transfer of MB/MS onto TCP as cells shed from the aggregate (Fig. 2*l*). The retention of dye indicates viability as the dye does not transfer from labeled to unlabeled cells and transfer may occur only when the membrane is disrupted. Therefore, the fluorescent signal is from intact cell membranes only, as the dye is weak in water if it were to leak out as a consequence of cell death.

Having established viable BMSC cultures in suspension using microspheres as scaffolds, we tested the ability of different polymers copolymerized with PLA microspheres to support cell culture. Four different polymers, alginate, dextran, gelatin, and pectin were used for BMSC culture. Alginate and gelatin are routinely used for adherent cell culture, and alginate hydrogels and
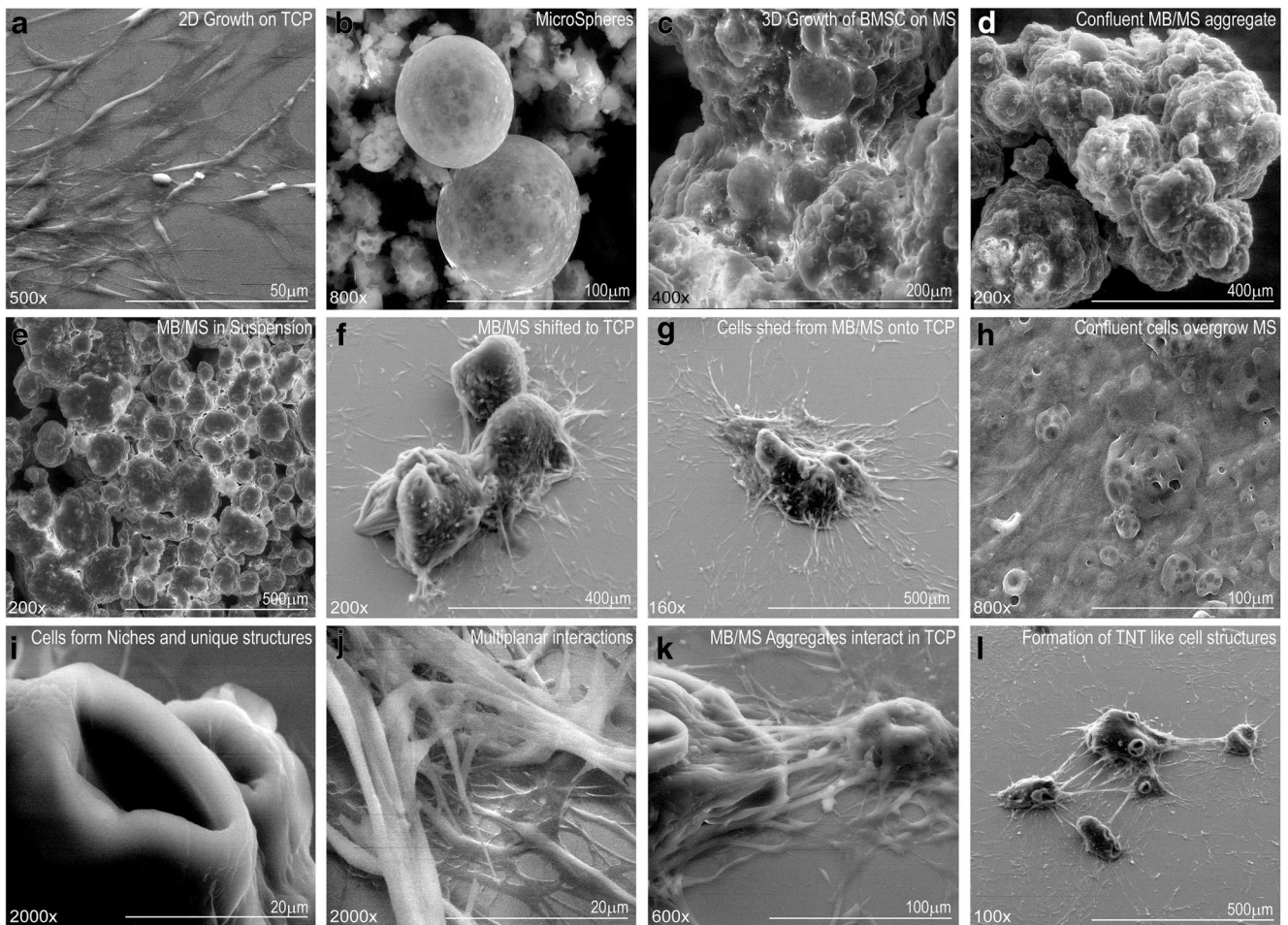
Figure 3. SEM analysis of MB/MS in culture. Scanning electron microscopy (SEM) was used to observe various stages in culture of mesoid body/microsphere (MB/MS). (*a*) SEM images showing standard 2D culture of BMSC. (*b*) Microsphere particles prior to culture. (*c*) 3D growth of MB incorporating MS (early stages of growth). (*d*) Confluent MB/MS where microspheres are completely encapsulated by cells. (*e*) Typical MB/MS culture with multiple aggregates of confluent MB/MS. (*f*) MB/MS transferred to TCP where cells attach to flat substrate. (*g*) Cells shed from MB/MS onto TCP and expand as monolayer. (*h*) Confluent cells degrade and grow over MS demonstrating retention of proliferative capacity. (*i–l*) Cell–cell interaction on multiple planes and formation of unique structures such as cell bridges (TNT-like structures or EP bridges) in MB/MS aggregates transferred to TCP.

microspheres have been employed in stem cell culture (Ashton *et al.* 2007). Dextran is often copolymerized with other molecules that improve its ability to serve as scaffolds (Lévesque and Shoichet 2006), while pectin is used in injectable biomaterials for bone tissue engineering (Munarin *et al.* 2011). The ability of these polymers to support BMSC adhesion for viable cell culture was measured using live imaging (Fig. 2*m–s*) and the automated tool of the Nikon Advanced Research software based on fluorescent signals. No significant difference in cell adhesion and aggregation of MB/MS was observed among the different coatings (Fig. 2*m–q*); however, gelatin and dextran-coated MS generated the largest MB/MS aggregates based on perimeter and area (Fig. 2*r, s*). While gelatin is a derivative of collagen and is known to support cell adhesion, dextran has limited cell-binding capabilities. These results suggest that dextran may be suitable for cell culture copolymerized with a PLA microsphere scaffold. Figure 2*t–y* shows scanning electron micrographs (SEMs) of

alginate, gelatin, and dextran microspheres taken under dry conditions and after 96 h in culture medium. It was observed that the MS maintained their structural integrity during the incorporation and aggregation of MB/MS and only begin to degrade after cells recede from the MS (Fig. 2*f*). Figure 2*t, v, x* also demonstrates the surface of the MS, where alginate MS shows a less porous structure as compared to gelatin or dextran MS. The porosity of the surface may play a role in cell adhesion and expansion, providing larger surface area for cells to attach to and colonize. This may contribute to the larger MB/MS aggregates formed by cells on gelatin and dextran MS (Fig. 2*r, s*). The diameter of an MS ranges from 25 to 100 μm with most MS averaging 50 μm in diameter (Fig. 2*t, v, x*). A typical MB/MS aggregate can incorporate between 5 and 10 MS when it reaches a confluent stage, while large aggregates can be composed of >20 MS (Fig. 2*e, k*).

To understand the surface morphology of cells on the MS and to reveal structural details of a typical MB/MS, SEM was

carried out on various stages of the development of the MB/MS (Fig. 3). Figure 3*a* shows a subconfluent monolayer culture on a TCP which is loaded onto gelatin MS (Fig. 3*b*) at 10^5 cells/ml. Figure 3*c* shows cells incorporating and growing over the microspheres, forming MB/MS until the cells are confluent (Fig. 3*d*). Typical MB/MS aggregates in suspension (Fig. 3*e*) can be collected by a wide mouth pipette and transferred to a cell-binding surface such as TCP, where cells anchor the MB/MS to the plate (Fig. 3*f*). Similar to explant culture, the cells shed from the aggregate and onto the TCP and resume proliferation (Fig. 3*g*). Figure 3*h* shows a confluent layer of cells overgrowing and degrading the microspheres which lose structural integrity and embed within the cell layer. Figure 3*i–l* shows the 3D pattern of growth of cells and their interaction on multiple planes. The adherent MB/MS aggregates interact and form cellular "bridges" which is not observed in the suspension culture (Fig. 3*k*). These aggregates form structures similar to tunneling nanotubes (TNTs) which are extensions that cells use to traffic signals and nutrients under conditions of stress (Zani and Edelman 2010; Zhang 2011). However, the extensions seen between MB/MS aggregates are larger and likely composed of cells. The lack of such cellular bridges in MB/MS in suspension maybe due to reduced cell proliferation. Space is a stimulus for cell proliferation, and when the MB/MS attach to the plate, cells may receive fresh signals to divide, producing these cellular bridges between aggregates. These cell bridges, or TNT, have been shown to be F-actin-rich structures that provide membrane continuity between connected cells and transport cellular components between them (Gurke *et al.* 2008). These structures may be vital to long-range cell-to-cell communication (Gurke *et al.* 2008; Zani and Edelman 2010). From the SEM experiments, it was observed that cell bridges between MB/MS aggregates were considerably large (Fig. 3*k, l*). To rule out the possibility that larger aggregates degraded during sample preparation for SEM (fixation and serial dehydration with ethanol) and forming these structures, we checked for TNT-like structures or cell bridges in live, smaller MB/MS aggregates by phase contrast microscopy (Fig. 4*a–d*). Figure 4*a* show cell bridges between two MB/MS, which was commonly observed in our cultures, between expanding cells from different MB/MS-establishing bridges. A cell bridge is shown in Fig. 4*b* which extends in length over 100 μm. Figure 4*c* shows large cell bridges between MB/MS that are ~10 μm in diameter similar to the ones observed by scanning electron microscopy (Fig. 4*d*) which suggests that these formations are induced by cells. These cell bridges are likely epithelial (EP) bridges that have been shown to be
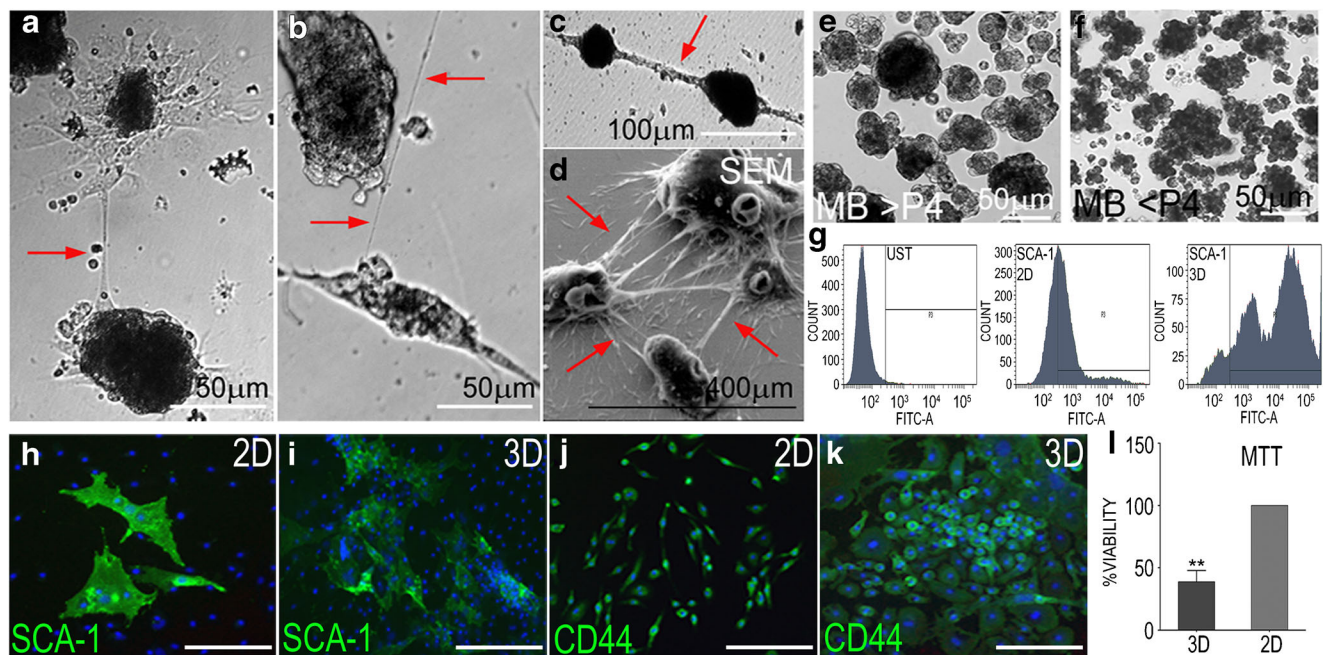

Figure 4. Intercellular communication, viability, and preservation of stem cell potency. Cellular functions and features are altered in MB/MS and MB cultures that form unique structures for intercellular communication and show reduced proliferation and retain stem cell potency (marker expression). (*a, b*) Phase contrast micrograph showing "cell bridges" between islands of MB/MS with varying diameters. *Red arrows* indicate the linking structures. (*b*) A tunneling nanotube-like structure connecting multiple islands of MB/MS. (*c*) EP bridges (epithelial bridges) between MB/MS of larger diameter connecting multiple MB/MS. (*d*) SEM image showing EP bridges between islands of MB/MS, typically forming over the substratum or monolayer of cells. (*e, f*) Passage number affects morphology of MB. Higher passage cells form cohesive spheroids (*e*) unlike lower passage number cells that form clusters (*f*). (*g*) Flow cytometric analysis showing retention of Sca-1 marker in 3D cultures compared with 2D Sca-1 marker expression. (*h–k*) Comparative ICC for Sca-1 and CD44 markers on 2D and 3D cultures. (*l*) MTT assay to quantify cell proliferation in 3D and 2D cultures (**p value 0.001 to 0.01).

structurally distinct from other cellular channels and mediate migration of cells between cell masses (Zani and Edelman 2010). EP bridges are structurally identical to the cell bridges observed in the MB/MS cultures (Figs. 3k, l and 4a–d). The length of the bridges suggest that these formations are EP bridges and not TNT as EP bridge diameters and lengths range from 1 to 20 μm in width and bridge connections extend from 25 μm to 1 mm in length (Zani and Edelman 2010) identical to the extensions observed in our cultures. The defining feature of EP bridges and TNT is that these structures make no contact with the monolayer of cells underneath and form over the substratum (Zani and Edelman 2010) identical to the structures present in MB/MS cultures (Fig. 4d). Figure 4e, f demonstrates the morphology of mesoid bodies that is determined by the passage number of BMSC. Cells over passage 4 formed cohesive spheroids where individual cells were not distinguishable (Fig. 4e), while cells under passage 4 formed clusters of cells (Fig. 4f). It was also observed that with increasing passage, the cells proliferated faster, and by passage 8, the BMSC lose expression of significant stem cell markers (Supplementary Fig. 1A).

The formation of cohesive spheroids may be related to the proliferative capacity of the cell as embryoid bodies have a similar cohesive structure and ESC have a significant rate of cell division (Itskovitz-Eldor et al. 2000). The lower passage cells have relatively lesser proliferative capacity, and this may prevent the formation of similar spheroids. The clusters still provide multiplanar interaction for cells, and the structure maybe indicative of stem cell potency. Passage number plays an important role in mesenchymal stem cell differentiation as studies have shown that P4 rat MSC expressed cardiomyocyte associated markers after treatment with 5-azacytidine while P1 and P8 cells do not (Zhang et al. 2005). Similarly, cell passage affects osteogenic ability of rat mesenchymal stem cells (Li et al. 2015). To verify retention of stem cell potency in MB/MS, we checked for the presence of the Sca-1 marker which is a good indicator of regenerative potential (Welm et al. 2002) (Fig. 4g). The Sca-1 marker is not expressed on all cells in the BMSC population, but the MB/MS show a reasonable number of cells that are positive and also appear to contain cells of different sizes that distinctly express the marker. However, the cell count is lower than TCP control as cells do not proliferate in the MB/MS due to the relatively reduced surface area. Cell proliferation is lower in MB/MS cultures but such cells are viable and resume proliferation when the MB/MS are shifted to TCP surfaces (Figs. 2e and 3h). In addition, these shifted MB/MS retain stem cell markers as shown in Fig. 4h–k, and the expression levels of Sca-1 and CD44 proteins appear distinctly higher in shifted MB/MS cells. MSC lose distinguishing markers with increasing passages and differentiation potential because of contamination of cultures with mature cells including fibroblasts that gradually replace MSC (Halfon et al. 2011) and the stem cell

microenvironment. An MTT assay was used to assess cell metabolism to indicate difference in levels of cell proliferation between a TCP culture and MB/MS culture which were initially seeded with the same number of cells (Fig. 4l). MB/MS reduce proliferation of potent cells and maintain the stem cell niche in addition to providing a highly conducive environment for cell signaling which may be very useful in directed differentiation for in vivo transplantation.

Differentiation of BMSC in 2D monolayer and 3D cultures. Adipogenesis in scaffold-free and scaffold-assisted suspension culture. BMSC can differentiate into multiple lineages, and as MB/MS appear to modulate important biological functions such as cell proliferation, cell morphology, marker expression, and formation of cell–cell communication structures, cell differentiation may also be affected. Adipogenesis from mesenchymal stem cells has been standardized by chemical induction (Contador et al. 2015) and is quantifiable by basic colorimetric analysis. Adipogenesis is also a process that can be regulated by major signaling pathways such as MAPK (Zang et al. 2013) which can be influenced by the MB/MS microenvironment. Figure 5a, c, e shows untreated monolayer, MB/MS, and MB, while b, d, f shows adipogenic induction medium (AIM)-treated cultures. The accumulation of triglycerides (TGA) or lipid droplets is indicative of adipocytes (Fig. 5b) (Kuri-Harcuch et al. 1978). These oval phase bright structures are clearly visible in the MB/MS on the periphery of the aggregates (Fig. 5d) as well as in the MB (Fig. 5f). No TGA is seen in untreated samples (Fig. 5a, c, e). Figure 5g, h shows untreated and AIM-treated MB, respectively, shifted to TCP where the TG accumulation is visible in expanding cells. The TGA is increased in the core of the MB which becomes apparent as the MB recedes into the plate and cells migrate away, allowing the visualization of these phase bright structures (Fig. 5h).

Having established that adipogenic differentiation can be induced in MB/MS and MB, ORO was used to quantify the lipid droplet (LD) or TG accumulation (Mehlem et al. 2013). Figure 5i–l shows untreated TCP, AIM-treated TCP, and AIM-treated MB/MS and MB, respectively, stained with ORO. ORO-stained LD is visibly high in MB/MS and MB (Fig. 5k, l), while TCP cultures also show stained lipid droplets indicating adipocytes. Interestingly, ORO uptake also confirmed mature, large LD in MB/MS and MB, while TCP cultures showed smaller LD. To confirm adipogenesis within the core of the MB, lipid droplet formation was qualitatively assessed by Nile red, a vital stain that has specificity for lipid droplets and can be detected by florescence microscopy when cells are viewed for yellow-gold fluorescence (Greenspan et al. 1985). Figure 5m, n shows Nile red-positive adipocytes at the core of the MB and in its peripheral, expanding monolayer. To quantify and compare adipogenesis within 2D and 3D growth, adipocytes from TCP, MB, and MB/MS were
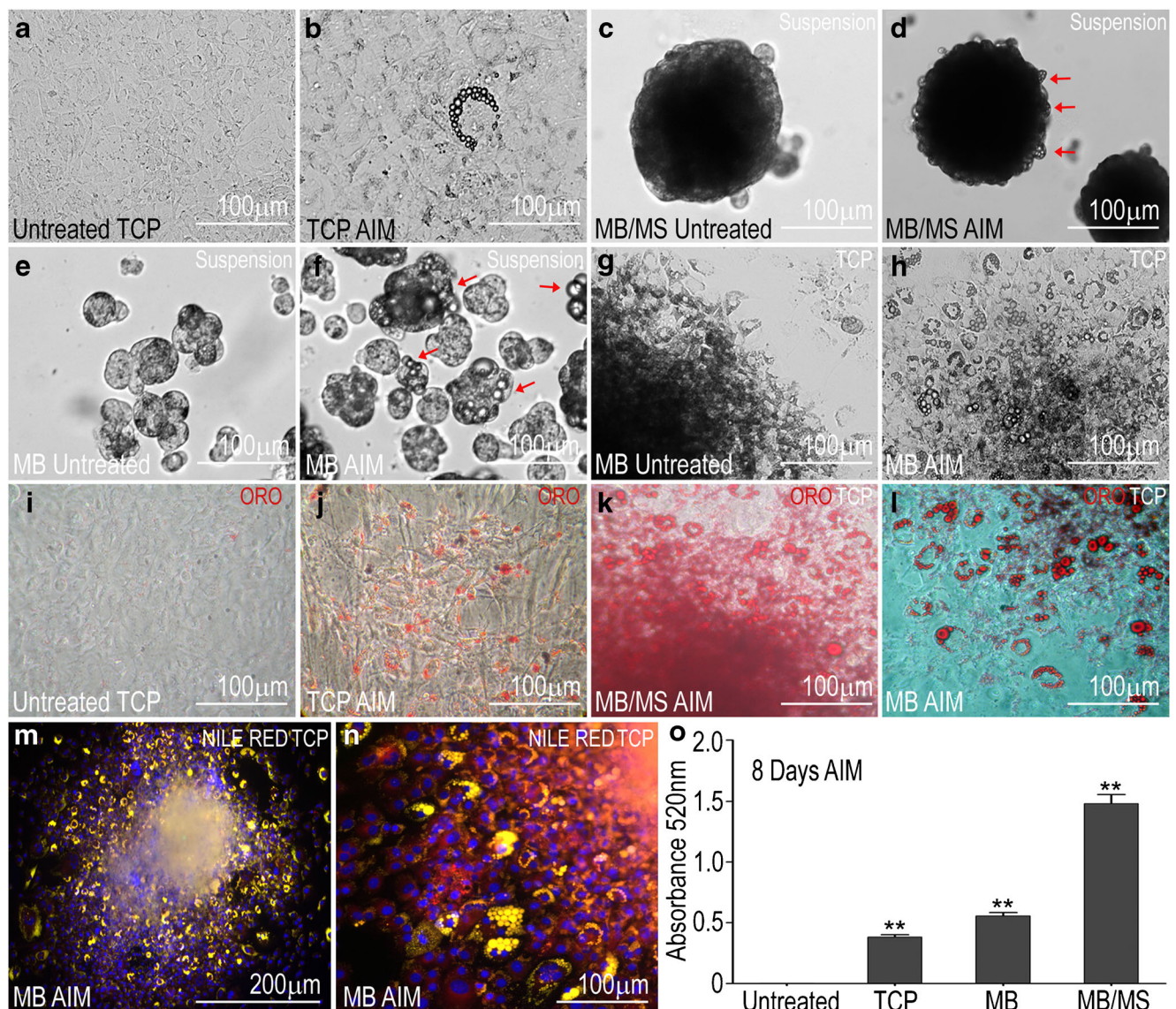
Figure 5. Adipogenic differentiation in MB and MB/MS cultures in suspension. Adipogenic differentiation (by adipogenic induction medium (AIM)) in MB and MB/MS cultured in suspensions showing triglyceride accumulation (TGA). (*a, c, e*) Control (untreated) TCP, MB/MS, and MB. (*b, d, f*) AIM induction in TCP, MB/MS, and MB showing TGA. (*g, h*) Untreated MB and AIM-treated MB transferred to TCP with AIM-treated MB showing TGA in cells shed from aggregate. (*i–l*) Oil Red O (ORO) staining in untreated TCP, treated TCP, treated MB/MS, and treated MB, respectively. (*m, n*) Nile red staining for treated MB transferred to TCP (high and low magnification revealing TGA in core of MB). (*o*) Quantification of ORO accumulation in lipid droplets at 520 nm comparing untreated TCP with treated TCP, MB, and MB/MS (**p value 0.001 to 0.01).

stained with ORO and the dye was extracted from the lipid droplets. Figure 5*o* shows absorbance readings at 520 nm of ORO extracts from 2D and 3D cultures treated with AIM for 8 d. The highest uptake of ORO was recorded in MB/MS which showed a ~2-fold difference over TCP and MB. This is significant as the number of cells in TCP was higher as MB and MB/MS cells do not proliferate and adipogenesis was noted earlier in 3D culture than in 2D. The higher dye uptake regardless of lower cell number can be attributed to mature adipocytes with greater triglyceride accumulation. Adipogenesis in 3D cultures of BMSC as reported here

indicates efficient and perhaps an enhanced differentiation potential over traditional monolayer cultures. The number of cells in a population that have committed to differentiation is probably higher in 3D culture. This may be due to the maintenance of potent stem cells within the non-proliferative environment of the MB or MB/MS.

Adipogenesis in scaffold-free, rotating cell culture. The use of a scaffold is suitable for in vitro directed differentiation of BMSC; however for transplantation and in vivo applications, a scaffold-free culture such as MB would be more appropriate

as there would be no concerns about residual scaffold or degradation of scaffold. In addition, MB shows higher differentiation potential than traditional monolayer culture and still possesses the same transplantable advantage of an MB/MS. To increase the efficiency of differentiation in MB cultures, a RCCS was used. An RCCS is a rotating wall vessel that was developed by NASA to simulate reduced gravity for cell cultures (Ferrarini et al. 2013; Morabito et al. 2014) which also generates 3D cell aggregates identical to the mesoid bodies in our study. The shear-free culture and constant free fall cancel the force of gravity on suspended cell cultures inside the vessel (known as the high-aspect rotating vessel (HARV)) and serves as an additional parameter that could influence differentiation efficiency or potential. Figure 6a shows a 10 ml HARV on a RCCS set to rotate at 27 rotations per minute (rpm) inside an incubator. Figure 6b shows static control (TCP monolayer) and RCCS-generated MB that is on average, 50 μm in diameter. Unlike larger MB generated in

suspension, RCCS-generated MB did not exceed 50–75 μm in our cultures. MB was formed based on vessel rpm, which influenced the rate of aggregation and viability of cells in the MB. An MTT assay was carried out to quantify cell proliferation in RCCS MB which showed higher proliferation at 27 rpm (Fig. 6c). The trend of slower proliferation similar to suspension MB is continued in the RCCS culture with static cultures being highly proliferative. A flow cytometry analysis of cell cycle of static BMSC and dissociated cells from RCCS MB showed a lower population of cells within the G0G1 phase in MB-derived cells (Fig. 6d). The sub-G0 population is likely from the mechanical and enzymatic dissociation of MB during sample preparation for flow cytometry as non-dissociated RCCS MB generate viable, expanding cells when shifted to TCP (qs demonstrated in CFU and BRDU assay for proliferative potential of RCCS MB, Supplementary Fig. 1B, C).
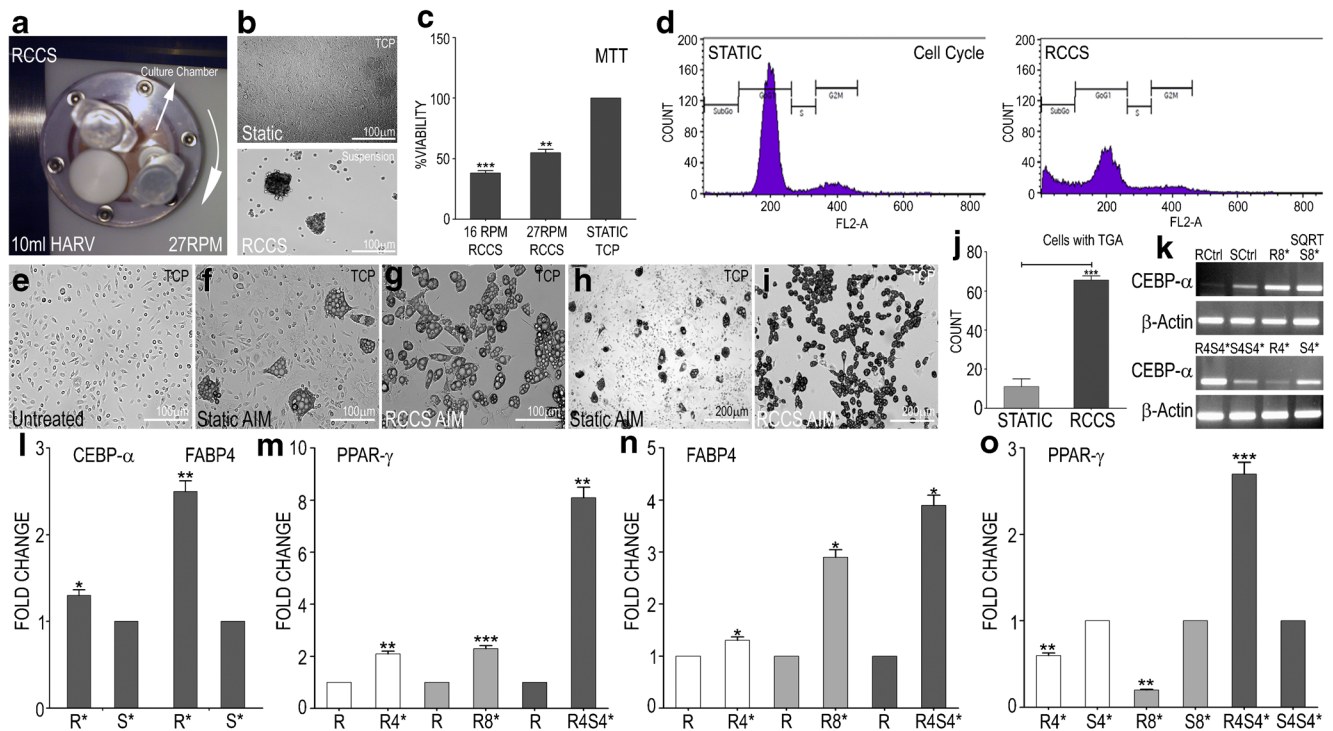

Figure 6. Adipogenic differentiation of MB cultures in RCCS. Culture of cells in the RCCS introduces constant free fall (reduced gravity) that could influence differentiation. (a) High-aspect ratio vessel (HARV) run at 27 rpm in a rotating cell culture system (RCCS) housed within a CO$_2$ incubator. (b) Static monolayer control and MB formed in RCCS. (c) MTT assay to quantify cell proliferation in RCCS at 16, 27 rpm, and static cultures. (d) Cell cycle analysis with PI for static and RCCS cultures showing difference in G0G1 phase. (e, f, g) Untreated TCP, AIM treatment in static conditions (TCP), and AIM treatment in RCCS MB transferred to TCP. (h, i) Low magnification micrograph showing increased triglyceride accumulation in AIM-treated RCCS MB transferred to TCP cultures. (j) Comparison of total count of cells with TGA between static monolayer and RCCS MB cultures showing higher number of cells committed to adipogenic differentiation in RCCS MB (p value

<0.0001). k SQRT-PCR for CEBPα gene expression under AIM treatment using three protocols. Asterisk indicates AIM treatment; R RCCS MB, S static TCP, RS transferred from RCCS to static TCP. Number indicates days in culture or treatment. Gene expression is highest in S8* (static, AIM treated for 8 d) and R4S4* (RCCS MB culture for 4 d without treatment, transferred to static TCP and AIM treated for 4 d; see densitometry analysis of SQRT-PCR in graph in Supplementary Fig. 1E). l CEBPα and FABP4 gene expression quantified by real-time PCR. (m, n, o) Real-time PCR for gene expression levels of central factors in adipogenesis of RCCS MB and static cultures using three protocols (asterisks over error bars in graphs represent statistical significance; *p value 0.01 to 0.05, **p value 0.001 to 0.01, ***p value 0.0001 to 0.001).

Adipogenesis from BMSC in the RCCS was carried out with multiple protocols which included "priming" the cells in the RCCS followed by AIM induction and routine AIM induction in RCCS. Static controls were treated for identical time periods. Figure 6e shows adipogenic induction in static monolayer and RCCS MB shifted to TCP. Figure 6e, f shows untreated static control and AIM-induced static BMSC after 10 days, respectively. Figure 6g shows RCCS MB shifted to TCP after 4 d followed by AIM induction for 6 d. Figure 6h, i is lower objective micrographs to show extent of adipogenesis in static and RCCS MB cultures. Cultures of RCCS MB shifted to TCP clearly show higher number of adipocytes as well as much more efficient differentiation of cells into the adipogenic lineage. As the micrographs show, the number of differentiated cells over undifferentiated is distinctly higher in RCCS MB despite lower number of cells in culture (Fig. 6h, i). The percentage of cells that is committed to adipocyte conversion in RCCS MB over static control shows efficient differentiation in 3D as confirmed by the statistically significant count of cells with TGA in RCCS MB over static (Fig. 6j, Supplementary Fig. 1D).

We report that the priming of cells for adipogenesis in the RCCS prior to AIM induction improves the efficiency of differentiation as demonstrated in Fig. 6e–j by validation with semiquantitative and real-time PCR analysis of important genes involved in adipogenesis such as central adipogenic factors, peroxisome proliferator-activated receptor γ (PPARγ), CCAAT-enhancer binding protein α (C/EBPα), and fatty acid-binding protein 4 (FABP4) (Suh et al. 2015; Tekkatte et al. 2012). Figure 6k shows CEBPα gene expression in BMSC through three adipogenic induction programs applied in RCCS and static cultures. In the first protocol, a basal level expression of CEBPα was present in untreated static BMSC and RCCS cultures (<static expression levels) after 8 days. AIM induction in RCCS and static for 8 d (R8* and S8*) shows a considerable increase in gene expression indicating adipogenesis with similar expression levels in both cultures. The second protocol involved AIM induction for 4 days on MB shifted to TCP after 4 d in the RCCS without treatment. CEBPα expression was significantly higher in R4S4* as compared to S4S4*, the static control. The third protocol showed lower levels of CEBPα expression in RCCS (R4* < S4*) indicating that AIM induction for 4 d in RCCS produced lesser adipogenesis than AIM-induced static cultures (Supplementary Fig. 1E) although, a 4-d AIM induction period may be too short to quantify adipogenesis. The overall gene expression of adipogenic markers CEBPα and FABP4 are higher in RCCS MB cultures than static as demonstrated by RT-PCR (1.3 and 2.5-fold, Fig. 6l). The trend of higher gene expression using the protocol of 4-day priming in RCCS prior to AIM induction continued in Pparg and FABP4 real-time PCR analysis (8-fold and 3.9-fold, respectively, Fig. 6m, n). Pparg gene expression was

2.7-fold higher in treated RCCS MB than treated static cultures under AIM induction (Fig. 6o) which is highly significant as Pparg is a central adipogenic factor and is part of many signaling networks (Farmer 2005). Cell shape and cytoskeletal tension have been shown to influence lineage commitment of MSC (McBeath et al. 2004), and the lack of gravity and its effect on cell morphology and cellular functions may increase the differentiation potential of these cells, which is seen even after they are expanded as a monolayer after induction.

Osteogenic differentiation. As observed in adipogenesis, differentiation potential is higher in 3D cultures of BMSC, and this is significantly enhanced when MB are shifted to TCP and allowed to expand as monolayer. Many cues in the local tissue microenvironment regulate commitment of BMSC into mesenchymal lineages such as cell shape. Human MSCs that were allowed to adhere, flatten, and spread underwent osteogenesis upon induction while unspread, round cells underwent adipogenesis (McBeath et al. 2004). These lineage differentiations were mediated by endogenous RhoA conditional on a round or spread shape. Therefore, a protocol of treating BMSC in MB suspensions with osteogenic induction medium (OIM) for 4 days followed by expansion in TCP as monolayer with continued OIM administration for up to 14 d was applied, allowing the cells to spread and flatten out during differentiation. Figure 7a, d shows untreated TCP and untreated MB shifted to TCP, respectively. Figure 7b, e shows OIM induction in TCP and MB shifted to TCP after 14 d with cultures demonstrating mineralization characteristic of osteogenic differentiation in vitro. Lower objective micrographs of OIM-induced TCP and MB cultures clearly show dense mineralization in MB cultures over TCP cultures (Fig. 7c, f). Similar to adipogenesis, a larger number of cells in MB cultures commit to osteogenesis producing dense mineralization whereas TCP cultures show a considerable percentage of non-committed cells under identical induction conditions.

Cardiomyogenic differentiation. Studies have reported the derivation of contracting cardiomyocytes from MSC by induction with 5-azacytidine (Makino et al. 1999; Balana et al. 2006). However, administration of 5-aza to BMSC in TCP did not generate functional cardiomyocytes in our study. Real-time PCR analysis for cardiac marker GATA4 only showed a small increase in gene expression (0.64 log FC) as compared to control cells—untreated BMSC, while GATA4 gene expression in the neonatal mouse heart was much higher (7.5 log FC) in comparison to the control cells (Fig. 7g). In order to increase differentiation, BMSC isolation and culture was modified to enrich the population of Sca-1$^+$ cells. Sca-1$^+$ populations have been shown to have increased regenerative potential compared with Sca-1$^-$ cells (Welm et al. 2002), and the Sca-1$^+$ population in the adult heart differentiates into beating cardiomyocytes (Matsuura et al. 2004). Figure 7h shows no
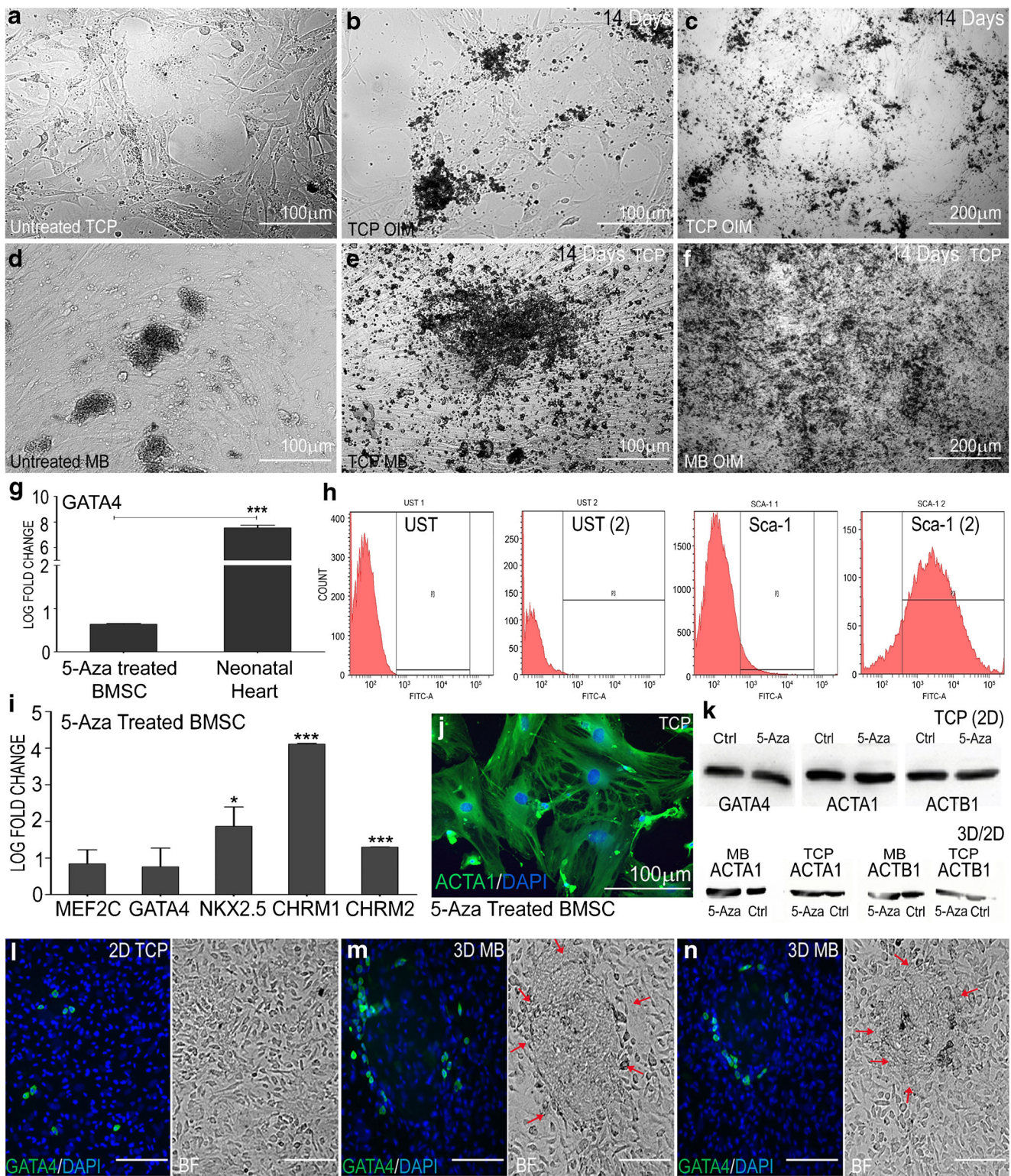
expression of Sca-1 in BMSC cultures isolated by basic 48-h plating procedure; however, a modified protocol generated cultures with small populations of Sca-1$^+$ cells (Fig. 7*h*, Isolation and culture of MSCs section). In addition to Sca-1$^+$ expression, lower passage cells were used for cardiomyogenic

differentiation. 5-Aza treatment on Sca-1$^+$ cultures improved expression of cardiac markers MEF2C, GATA4, NKX2.5, CHRM1, and CHRM2 with respect to untreated control (Fig. 7*i*), and ACTA1 was detectable in ICC (Fig. 7*j*). However, the stromal cell shape was retained,

◀ **Figure 7.** Osteogenic and cardiomyogenic differentiation of MB cultures. Osteogenic and cardiomyogenic lineage was carried out by treating suspension cultures of MB with induction medium and expanding as monolayer. (*a–f*) Osteogenic differentiation of MB expanded as monolayer on TCP following OIM induction. (*a, d*) Untreated monolayer and untreated MB expanded as monolayer. *b, e* Mineralization in monolayer and MB expanded as monolayer indicating osteogenic differentiation of BMSC. (*c, f*) Lower objective phase contrast micrographs showing robust mineralization in MB expanded as monolayer in OIM in comparison to lesser mineralization in standard monolayer. (*g*) Gene expression of GATA4 in 5-azacytidine-treated BMSC (0.64 log FC) and neonatal mouse heart (7.5 log FC) compared to control cells—untreated BMSC demonstrated in log2 fold change. 5-Aza treatment was carried out on BMSC isolated with original 48-h protocol. (*h*) Modified protocol showed increase in Sca-1 expression over original 48-h protocol. (*i*) Log fold change in gene expression of cardiac markers in 5-aza-treated BMSC over control cells—untreated BMSC, isolated by modified protocol (log2 fold change of 5-aza-treated BMSC gene expression with respect to untreated control BMSC; *$*p$ value 0.01 to 0.05, $**p$ value 0.001 to 0.01, $***p$ value 0.0001 to 0.001). (*j*) ICC for alpha sarcomeric actin 1 (ACTA1) in 5-aza-treated BMSC isolated by modified protocol shows protein expression with retention of stromal morphology. (*k*) Western blotting for GATA4 and ACTA1 in 5-aza treated and untreated BMSC monolayer shows protein expression in both cultures. (*Lower panel*) Western blotting for ACTA1 protein in 5-aza-treated MB and TCP cultures shows very small increase in ACTA1 expression in treated MB (see densitometry analysis of WB in graph in Supplementary Fig. 1F). (*l, m, n*) ICC for GATA4 in TCP and MB expanded as monolayer in TCP shows expression in both cultures with GATA4 expression concentrated around MB.

and no instances of contraction were observed. Cardiomyogenic differentiation of MSC is a complex process, and studies report that differentiation cued BMSC express cardiomyogenic proteins but do not generate functional cardiomyocytes (Siegel *et al.* 2012). Untreated bone marrow-derived MSC also express cardiac-specific markers and retain the stromal phenotype without becoming functional cardiomyocytes in vitro (Rose *et al.* 2008). Makino et al. also describe the expression of cardiac markers in untreated (with 5-aza) MSC in their study on generation of a cardiomyogenic cell line from BMSC (Makino *et al.* 1999). Figure 7*k* shows western blotting for cardiac markers GATA4 and ACTA1 which demonstrated protein bands in both 5-aza treated and untreated cultures with very little change in expression levels. Figure 7*k* (bottom panel) shows western blotting for ACTA1 under 3D and 2D conditions (MB shifted to TCP and TCP, respectively) where an increase in 5-aza-treated MB can be observed (Supplementary Fig. 1*F*). GATA4 expression was detected by ICC in both cultures of 5-aza-treated TCP and MB shifted to TCP (Fig. 7*l, m, n*). Functional cardiomyogenic differentiation of BM-derived MSC is a rare event (Siegel *et al.* 2012), and therefore, quantification of efficiency of cardiomyogenic differentiation in MB and monolayer cultures is not conclusive. Although beyond the scope of the current study, other mechanisms of cardiomyogenic induction in MSC may yield quantifiable differentiation in 3D cultures.

In conclusion, spheroid culture of BMSC as scaffold-free MB or as aggregates with PLA microspheres provides a physiologically relevant alternative to standard 2D culture on TCP. 3D culture allows the maintenance of viable BMSC, interaction on multiple planes, and formation of specialized cell structures such as epithelial cell bridges and retention of the Sca-1 stem cell marker. The formation of structures similar to tunneling nanotubes and EP bridges between MB/MS aggregates in these cultures makes them functional models for in vitro studies on complex cell–cell and cell–matrix interactions. This is the first report of intercellular communication structures such as EP bridges between scaffold-supported 3D cell aggregates. Significantly, differentiation of BMSC into the adipogenic lineage is enhanced in MB/MS and MB cultures over standard TCP cultures, while expansion of mesoid bodies on 2D substrates improves osteogenesis. Although cardiomyogenesis was inconclusive and not quantifiable, expression of cardiac markers under both 3D and 2D culture conditions suggests that multilineage potential is preserved. Cardiomyogenic induction with other external differentiation cues in 3D culture may yield functional cardiomyocytes. Adipogenesis is of major relevance to metabolic diseases such as obesity, and understanding adipogenic differentiation will enable researchers to improve function of diseased adipocytes or replace those cells (Unger *et al.* 2010). Enhanced adipogenesis was observed in all three methods of 3D culture. This is the first report of an optimized protocol that efficiently derives and enhances adipogenesis using a rotating cell culture system. The priming of BMSC in RCCS 3D cultures can enhance and optimize stem cells for use in regenerative therapies involving cell replacement or augmentation of function.

References

Ashton RS, Banerjee A, Punyani S, Schaffer DV, Kane RS (2007) Scaffolds based on degradable alginate hydrogels and poly(lactide-co-glycolide) microspheres for stem cell culture. Biomaterials 28: 5518–5525. doi:10.1016/j.biomaterials.2007.08.038

Balana B, Nicoletti C, Zahanich I, Graf E, Christ T, Boxberger S, Ravens U (2006) 5-Azacytidine induces changes in electrophysiological properties of human mesenchymal stem cells. Cell Res 16:949–960. doi:10.1038/sj.cr.7310116

Baraniak PR, McDevitt TC (2012) Scaffold-free culture of mesenchymal stem cell spheroids in suspension preserves multilineage potential. Cell Tissue Res 347:701–711. doi:10.1007/s00441-011-1215-5

Bloom AB, Zaman MH (2014) Influence of the microenvironment on cell fate determination and migration. Physiol Genomics 46:309–314. doi:10.1152/physiolgenomics.00170.2013

Bonab MM, Alimoghaddam K, Talebian F, Ghaffari SH, Ghavamzadeh A, Nikbin B (2006) Aging of mesenchymal stem cell in vitro. BMC Cell Biol 7:14. doi:10.1186/1471-2121-7-14

Cha H-MM, Kim S-MM, Choi Y-SS, Kim D-II (2015) Scaffold-free three-dimensional culture systems for mass production of periosteum-derived progenitor cells. J Biosci Bioeng. doi:10.1016/j.jbiosc.2014.12.019

Contador D, Ezquer F, Espinosa M, Arango-Rodriguez M, Puebla C, Sobrevia L, Conget P (2015) Dexamethasone and rosiglitazone are sufficient and necessary for producing functional adipocytes from mesenchymal stem cells. Exp Biol Med (Maywood). doi:10.1177/1535370214566565

Dominici M, Le Blanc K, Mueller I, Slaper-Cortenbach I, Marini F, Krause D, Deans R, Keating A, Prockop DJ, Horwitz E (2006) Minimal criteria for defining multipotent mesenchymal stromal cells. The International Society for Cellular Therapy position statement. Cytotherapy 8:315–317. doi:10.1080/14653240600855905

Farmer SR (2005) Regulation of PPARγ activity during adipogenesis. Int J Obes Relat Metab Disord (Lond) 29:S13–S16. doi:10.1038/sj.ijo.0802907

Ferrarini M, Steimberg N, Ponzoni M, Belloni D, Berenzi A, Girlanda S, Caligaris-Cappio F, Mazzoleni G, Ferrero E (2013) Ex-vivo dynamic 3-D culture of human tissues in the RCCS™ bioreactor allows the study of Multiple Myeloma biology and response to therapy. PLoS ONE 8:e71613. doi:10.1371/journal.pone.0071613

Greenspan P, Mayer EP, Fowler SD (1985) Nile red: a selective fluorescent stain for intracellular lipid droplets. J Cell Biol 100:965–973

Gurke S, Barroso J, Gerdes H-H (2008) The art of cellular communication: tunneling nanotubes bridge the divide. Histochem Cell Biol 129:539–550. doi:10.1007/s00418-008-0412-0

Halfon S, Abramov N, Grinblat B, Ginis I (2011) Markers distinguishing mesenchymal stem cells from fibroblasts are downregulated with passaging. Stem Cells Dev 20:53–66. doi:10.1089/scd.2010.0040

Itskovitz-Eldor J, Schuldiner M, Karsenti D, Eden A, Yanuka O, Amit M, Soreq H, Benvenisty N (2000) Differentiation of human embryonic stem cells into embryoid bodies compromising the three embryonic germ layers. Mol Med 6:88–95

Kuri-Harcuch W, Wise LS, Green H (1978) Interruption of the adipose conversion of 3T3 cells by biotin deficiency: differentiation without triglyceride accumulation. Cell 14:53–59

Lei IL, Bu L, Wang Z (2015) Derivation of cardiac progenitor cells from embryonic stem cells. J Vis Exp. doi:10.3791/52047

Lévesque SG, Shoichet MS (2006) Synthesis of cell-adhesive dextran hydrogels and macroporous scaffolds. Biomaterials 27:5277–5285. doi:10.1016/j.biomaterials.2006.06.004

Li C, Wei G, Gu Q, Wen G, Qi B, Xu L, Tao S (2015) Donor age and cell passage affect osteogenic ability of rat bone marrow mesenchymal stem cells. Cell Biochem Biophys. doi:10.1007/s12013-014-0500-9

Makino S, Fukuda K, Miyoshi S, Konishi F, Kodama H, Pan J, Sano M, Takahashi T, Hori S, Abe H, Hata J, Umezawa A, Ogawa S (1999) Cardiomyocytes can be generated from marrow stromal cells in vitro. J Clin Invest 103:697–705. doi:10.1172/JCI5298

Matsuura K, Nagai T, Nishigaki N, Oyama T, Nishi J, Wada H, Sano M, Toko H, Akazawa H, Sato T, Nakaya H, Kasanuki H, Komuro I (2004) Adult cardiac Sca-1-positive cells differentiate into beating cardiomyocytes. J Biol Chem 279:11384–11391. doi:10.1074/jbc.M310822200

McBeath R, Pirone DM, Nelson CM, Bhadriraju K, Chen CS (2004) Cell shape, cytoskeletal tension, and RhoA regulate stem cell lineage commitment. Dev Cell 6:483–495

Mehlem A, Hagberg CE, Muhl L, Eriksson U, Falkevall A (2013) Imaging of neutral lipids by oil red O for analyzing the metabolic status in health and disease. Nat Protoc 8:1149–1154. doi:10.1038/nprot.2013.055

Morabito C, Steimberg N, Mazzoleni G, Guarnieri S, Fanò-Illic G, Mariggiò MA (2015) RCCS bioreactor-based modelled microgravity induces significant changes on in vitro 3D neuroglial cell cultures. BioMed Res Int 2015:1–14. doi:10.1155/2015/754283

Munarin F, Guerreiro SG, Grellier MA, Tanzi MC, Barbosa MA, Petrini P, Granja PL (2011) Pectin-based injectable biomaterials for bone tissue engineering. Biomacromolecules 12:568–577. doi:10.1021/bm101110x

Pittenger MF (2008) Mesenchymal stem cells from adult bone marrow. Methods Mol Biol 449:27–44. doi:10.1007/978-1-60327-169-1_2

Rose RA, Jiang H, Wang X, Helke S, Tsoporis JN, Gong N, Keating SC, Parker TG, Backx PH, Keating A (2008) Bone marrow-derived mesenchymal stromal cells express cardiac-specific markers, retain the stromal phenotype, and do not become functional cardiomyocytes in vitro. Stem Cells 26:2884–2892. doi:10.1634/stemcells.2008-0329

Sahoo SK, Panda AK, Labhasetwar V (2005) Characterization of porous PLGA/PLA microparticles as a scaffold for three dimensional growth of breast cancer cells. Biomacromolecules 6:1132–1139. doi:10.1021/bm0492632

Shyamsunder P, Vidyasekar P, Shukla A, Mohan S, Verma R (2013) Lowered expression levels of a tumor suppressor gene—caveolin-1 within dysregulated gene networks of Fanconi anemia. Gene 527:521–528. doi:10.1016/j.gene.2013.06.051

Siegel G, Krause P, Wöhrle S, Nowak P, Ayturan M, Kluba T, Brehm B, Neumeister B, Köhler D, Rosenberger P, Just L, Northoff H, Schäfer R (2012) Bone marrow-derived human mesenchymal stem cells express cardiomyogenic proteins but do not exhibit functional cardiomyogenic differentiation potential. Stem Cells Dev 21:2457–2470. doi:10.1089/scd.2011.0626

Soleimani M, Nadri S (2009) A protocol for isolation and culture of mesenchymal stem cells from mouse bone marrow. Nat Protoc 4:102–106. doi:10.1038/nprot.2008.221

Suh HJ, Cho SY, Kim EY, Choi H-SS (2015) Blockade of lipid accumulation by silibinin in adipocytes and zebrafish. Chem Biol Interact 227C:53–62. doi:10.1016/j.cbi.2014.12.027

Tekkatte C, Vidyasekar P, Kapadia N, Verma R (2012) Enhancement of adipogenic and osteogenic differentiation of human bone-marrow-derived mesenchymal stem cells by supplementation with umbilical cord blood serum. Cell Tissue Res 347:383–395. doi:10.1007/s00441-012-1328-5

Unger RH, Clark GO, Scherer PE, Orci L (2010) Lipid homeostasis, lipotoxicity and the metabolic syndrome. Biochim Biophys Acta 1801:209–214. doi:10.1016/j.bbalip.2009.10.006

Wagner W, Bork S, Lepperdinger G, Joussen S, Ma N, Strunk D, Koch C (2010) How to track cellular aging of mesenchymal stromal cells? Aging (Albany NY) 2:224–230

Weir C, Morel-Kopp M-C, Gill A, Tinworth K, Ladd L, Hunyor S, Ward C (2008) Mesenchymal stem cells: isolation, characterisation and in vivo fluorescent dye tracking. Heart Lung Circ 17:395–403. doi:10.1016/j.hlc.2008.01.006

Weiswald L-BB, Bellet D, Dangles-Marie V (2015) Spherical cancer models in tumor biology. Neoplasia 17:1–15. doi:10.1016/j.neo.2014.12.004

Welm BE, Tepera SB, Venezia T, Graubert TA, Rosen JM, Goodell MA (2002) Sca-1(pos) cells in the mouse mammary gland represent an enriched progenitor cell population. Dev Biol 245:42–56. doi:10.1006/dbio.2002.0625

Yamada K, Cukierman E (2007) Modeling tissue morphogenesis and cancer in 3D. Cell. doi:10.1016/j.cell.2007.08.006

Zang K, Wang J, Dong M, Sun R, Wang Y, Huang Y, Liu X, Li Y, Wang F, Yu M (2013) Brd2 inhibits adipogenesis via the ERK1/2 signaling pathway in 3T3-L1 adipocytes. PLoS ONE 8:e78536. doi:10.1371/journal.pone.0078536

Zani B, Edelman E (2010) Cellular bridges: routes for intercellular communication and cell migration. Commun Integr Biol 3:215–220

Zhang Y (2011) Tunneling-nanotube. Commun Integr Biol. doi:10.4161/cib.4.3.14855

Zhang F-B, Li L, Fang B, Zhu D-L, Yang H-T, Gao P-J (2005) Passage-restricted differentiation potential of mesenchymal stem cells into cardiomyocyte-like cells. Biochem Biophys Res Commun 336:784792. doi:10.1016/j.bbrc.2005.08.177